Journal of General Virology (2007), **88**, 196–206 **DOI** 10.1099/vir.0.82282-0

The nine C-terminal amino acids of the respiratory syncytial virus protein P are necessary and sufficient for binding to ribonucleoprotein complexes in which six ribonucleotides are contacted per N protein protomer

Thi-Lan Tran,[1]† Nathalie Castagné,[1]† David Bhella,[2] Paloma F. Varela,[3]‡ Julie Bernard,[1] Stefan Chilmonczyk,[1] Stefan Berkenkamp,[4] Vanessa Benhamo,[1] Katarina Grznarova,[1] Jeanne Grosclaude,[1] Claude Nespoulos,[5] Felix A. Rey[3]§ and Jean-François Eléouët[1]

Correspondence
Jean-François Eléouët
jean-francois.eleouet@jouy.inra.fr

[1]Unité de Virologie et Immunologie Moléculaires, INRA, 78350 Jouy-en-Josas, France

[2]Medical Research Council Virology Unit, Church Street, Glasgow G11 5JR, UK

[3]Laboratoire de Virologie Moléculaire et Structurale, UMR 2472-1157 CNRS-INRA and IFR 115, 1 Avenue de la Terrasse, 91198 Gif-sur-Yvette Cedex, France

[4]Institute of Medical Physics and Biophysics, Westfälische Wilhelms-Universität, Münster, Germany

[5]Unité de Biochimie et Structure des Protéines, INRA, 78350 Jouy-en-Josas, France

The respiratory syncytial virus (RSV) phosphoprotein (P) is a major polymerase co-factor that interacts with both the large polymerase fragment (L) and the nucleoprotein (N). The N-binding domain of RSV P has been investigated by co-expression of RSV P and N proteins in *Escherichia coli*. Pull-down assays performed with a series of truncated forms of P fused to glutathione *S*-transferase (GST) revealed that the region comprising the last nine C-terminal amino acid residues of P (233-DNDLSLEDF-241) is sufficient for efficient binding to N. Site-directed mutagenesis shows that the last four residues of this peptide are crucial for binding and must be present at the end of a flexible C-terminal tail. The presence of the P oligomerization domain (residues 100–160) was an important stabilizing factor for the interaction. The tetrameric full-length P fused to GST was able to pull down both helical and ring structures, whereas a monomeric C-terminal fragment of P (residues 161–241) fused to GST pulled down exclusively RNA–N rings. Electron-microscopy analysis of the purified rings showed the presence of two types of complex: undecamers (11N) and decamers (10N). Mass-spectrometry analysis of the RNA extracted from rings after RNase A treatment showed two peaks of 22 900 and 24 820 Da, corresponding to a mean RNA length of 67 and 73 bases, respectively. These results suggest strongly that each N subunit contacts 6 nt, with an extra three or four bases further protected from nuclease digestion by the ring structure at both the 5′ and 3′ ends.

Received 8 June 2006
Accepted 28 August 2006

INTRODUCTION

Respiratory syncytial virus (RSV) is a pneumovirus of the family *Paramyxoviridae* (Collins *et al.*, 2001). The 15 kb single-stranded RNA genome is encapsidated by the nucleocapsid (N) protein to form an RNase-resistant nucleocapsid of helical structure. This RNA–N complex acts as a template for replication and transcription by the polymerase complex of the virus, which includes the phosphoprotein (P), the large polymerase subunit (L protein) and the M2-1 and M2-2 co-factors. P, N and L constitute the minimal components required for virus RNA replication and transcription *in vitro* (Grosfeld *et al.*, 1995).

RSV P is a multifunctional protein capable of interacting with multiple partners. It forms homo-oligomers that are believed to be tetrameric (Asenjo & Villanueva, 2000) and

†These authors contributed equally to this work.

‡Present address: Laboratoire de Biologie, Synchrotron SOLEIL, L'Orme des Merisiers, Saint Aubin – BP 48, 91192 Gif-sur-Yvette Cedex, France.

§Present address: Unité de Virologie Structurale, Institut Pasteur, 28 rue du Docteur Roux, 75724 Paris Cedex 15, France.

has been shown to bind L (Khattar *et al.*, 2001a), N (García *et al.*, 1993) and M2-1 (Mason *et al.*, 2003). During genome transcription and replication, P is believed to position L on the RNA–N template and to help in translocating the polymerase complex along the helical nucleocapsid. By analogy to members of the *Paramyxovirinae* and *Rhabdoviridae*, P is also believed to play a chaperone role, maintaining newly synthesized N in a soluble form (N°) and delivering it to encapsidate specifically the virus genomic and anti-genomic RNAs (Kolakofsky *et al.*, 2004).

Human RSV (HRSV) P is 241 aa long and has been shown to be phosphorylated by cellular casein kinase II on several serine residues located towards the centre of the protein (at positions 116, 117 and 119), as well as in the C-terminal region (positions 232 and 237) of the molecule (Navarro *et al.*, 1991). Ser^{232} carries the main phosphorylation site (Barik *et al.*, 1995). The role of phosphorylation at the different sites remains to be clarified, as it is dispensable for genome replication (Lu *et al.*, 2002).

The oligomerization domain of RSV P has been mapped to the central part of the molecule, encompassing aa 120–150 (Castagné *et al.*, 2004), and an oligomeric trypsin-resistant fragment (fragment 'X') encompassing residues 104–163 has been identified (Llorente *et al.*, 2006). RSV P is predicted to contain a coiled-coil domain spanning residues 130–155 (Castagné *et al.*, 2004; Llorente *et al.*, 2006). The C-terminal region of P was shown to be important for interactions with N, as removal of the last 6 aa of the protein abolished this interaction (García-Barreno *et al.*, 1996). Several groups have confirmed the importance of this region for binding to N (Slack & Easton, 1998). Depending on the approaches used, internal regions were also found to be important for N–P interactions. The C-terminal 54 aa of HRSV P were found to be insufficient for N–P complex formation as assayed in the yeast two-hybrid system, and other regions necessary for N–P interactions were mapped to aa 132–168 and 161–180 for bovine RSV (Khattar *et al.*, 2001a). Within this region, temperature-sensitive mutations G172 and E176 were identified for HRSV P that could affect the N–P interactions (Lu *et al.*, 2002). Data from the study by Mason *et al.* (2003) suggested that the region spanning aa 120–160 – containing the oligomerization domain – is important for N binding. Finally, a region located at the N terminus of P has also been suspected to play a role in the N–P interaction (Mallipeddi *et al.*, 1996).

For *Rabies virus* (RV) and *Sendai virus* (SeV), belonging to the families *Rhabdoviridae* and *Paramyxoviridae*, respectively, two distinct N-binding regions have been mapped on P, the first corresponding to the RNA–N binding and located at the C terminus (Longhi *et al.*, 2003; Mavrakis *et al.*, 2004) and the second corresponding to N° binding and located at the N terminus (Curran *et al.*, 1995; Mavrakis *et al.*, 2006). However, for RSV, it has not been determined whether these two distinct N-binding regions exist.

We determined previously that co-expression of RSV N and glutathione *S*-transferase (GST)–P in *Escherichia coli* results in a complex containing the two proteins that can be isolated (Castagné *et al.*, 2004). In this work, we analysed these complexes further and showed that they are composed essentially of P associated with RNA–N complexes. We determined that a region containing the nine amino acid residues located at the most C-terminal part of P is sufficient for binding to RNA–N structures. This region is completely distinct from RNA–N-binding domains of other members of the order *Mononegavirales* that have been described previously.

METHODS

Plasmid construction. The pGEX-P and pET-N plasmids have been described previously (Castagné *et al.*, 2004). The P C-terminal deletion mutants were derived by introducing stop codons at the appropriate point in the coding sequence by using *Pfu* DNA polymerase with a QuikChange Site-Directed Mutagenesis kit (Stratagene) according to the manufacturer's instructions. N-terminal deletion mutants were obtained by PCR using appropriate primers (sequences available on demand) and *Pfu* DNA polymerase (Stratagene), then fused at the C terminus of *Schistosoma japonicum* GST by cloning in the pGEX-4T-3 vector (Amersham Biosciences) between the unique *Bam*HI and *Sma*I sites and just downstream of a thrombin-cleavage site. For constructions containing original or mutated P231–241 region, complementary antiparallel oligonucleotides were hybridized and inserted at the *Bam*HI/*Sma*I sites in the pGEX-4T-3 vector (detailed sequences are available on demand). We used the following notation: PΔN230 contains aa 230–241; PΔC230 contains aa 1–230; P82–208 contains aa 82–208. The integrity of all constructs was assessed by DNA sequencing.

Expression and purification of recombinant proteins from *E. coli*. *E. coli* BL21 (DE3) (Novagen) cells transformed with the pGEX-4T3-derived and pET-N plasmids were grown at 37 °C for 8 h in 1 l Luria–Bertani (LB) medium containing 100 μg ampicillin ml^{-1} and 50 μg kanamycin ml^{-1}. The same volume of fresh LB medium was then added and protein expression was induced by adding IPTG to the medium (final concentration, 0.33 mM). The bacteria were grown at 28 °C and harvested by centrifugation 15 h after induction. GST-fusion proteins were purified from the bacterial pellets as described previously (Castagné *et al.*, 2004). Identification of the polypeptides in polyacrylamide gels stained with Coomassie blue was done by MALDI-TOF as described previously (Castagné *et al.*, 2004).

Isolation and analysis of RNA from purified PΔN161–N complexes. One millilitre of glutathione–Sepharose 4B beads containing the GST–PΔN161–N complex-adsorbed protein complexes resuspended in an equal volume of PBS was mixed with an equal volume of phenol/chloroform, vortexed and centrifuged. The nucleic acid-containing aqueous layer was removed and RNA was precipitated with 2.5 vols ethanol, with the addition of 0.1 vol. 3 M sodium acetate at −70 °C. RNA was analysed by electrophoresis on an 8 M urea/polyacrylamide gel. RNA molecular mass standards were generated by *in vitro* transcription with T7 RNA polymerase using the pBlueScript vector digested by the following restriction enzymes (length of the transcripts is shown in parentheses): *Eco*RV (55 bases), *Eco*RI (63 bases), *Sma*I (73 bases), *Bam*HI (81 bases), *Xba*I (93 bases).

Mass-spectrometry analysis of RNA. For the mass-spectrometric analysis, a matrix-assisted laser desorption/ionization–time-of-flight

mass spectrometer with orthogonal ion extraction was used (MALDI-O-TOF). A detailed description of the instrument can be found in the study by Loboda *et al.* (2003). 3-Hydroxypicolinic acid (Fluka) was used as matrix and was dissolved to saturation in water/acetronitrile (3 : 1). For analysis, 1 μl matrix solution was pipetted together with 1 μl aqueous RNA sample (concentration, approx. 0.5–1 pmol μl^{-1}) and dried on a stainless-steel target. For the individual mass spectra, ions generated by around 500 lasershots were emitted from a nitrogen laser (337ND-Sx, Spectra Physics; wavelength 337 nm). The laser light was guided onto the target with a fibre of 100 μm core diameter, resulting in a spot size on the target of approximately 100 × 140 μm.

Transmission electron microscopy (TEM) of RSV N–RNA. Purified N–RNA complexes were imaged by negative-stain microscopy in a JEOL 1200 EXII transmission electron microscope operated at an accelerating voltage of 120 kV. For imaging by negative stain on continuous carbon, 5 μl protein suspension was loaded onto a freshly air glow-discharged carbon-coated 400-mesh copper TEM grid for approximately 30 s. This was then washed for 30 s in a 50 μl droplet of distilled H_2O and stained for 10 s in a 20 μl droplet of 2 % ammonium molybdate (pH 7.1). Grids were then drained and allowed to air-dry before imaging. Low-electron-dose micrographs were recorded at × 30 000 magnification at an approximate defocus of 1 μm on Kodak SO 163 film. For image processing, N–RNA rings were imaged on holey carbon support films. Protein suspension (5 μl) was loaded onto a freshly air glow-discharged Quantifoil holey carbon support film (R2/2 400 mesh copper grid; Quantifoil Micro Tools GmbH) for 10–20 s. This was then washed for 30 s in a 50 μl droplet of 0.1 % trehalose solution before staining in a 20 μl droplet of 5 % ammonium molybdate (pH 7.1) in 0.1 % trehalose. Grids were then drained and allowed to air-dry before imaging as above.

Image processing. Two-dimensional top-view averages were calculated from images of N–RNA rings produced by expression of PΔN161–N, purified by gel filtration and embedded in 5 % ammonium molybdate/0.1 % trehalose. Micrographs were digitized on a Nikon Super Coolscan 9000 ED CCD scanner at 4000 d.p.i. resolution, corresponding to a raster step size of 2.18 Å at the specimen scale. Two thousand two hundred and eleven top views of N–RNA rings were selected for analysis and excised into 128 × 128 pixel boxes by using X3D (Conway & Steven, 1999). Two-dimensional averages were calculated by using the EMAN image-processing package (Ludtke *et al.*, 1999). Six preliminary averages were determined, of which five revealed a ring-structure composition of 10 subunits. The sixth average, calculated from 263 raw images, appeared to comprise 11 subunits and was slightly larger in diameter; however, the spoke-like protrusions in this average were poorly defined. To determine more accurately the proportion of rings comprising 10 or 11 subunits and to improve the quality of averages, three models were used to classify each raw image by projection matching (multi-reference alignment). To generate these models, the best average, comprising 10 subunits per ring, was averaged according to C10 symmetry, whilst the larger 11-membered ring was subjected to both C10 and C11 averaging.

Kinetics of P–RNA–N interactions. Kinetics of GST–P and RNA–N interaction were followed by surface plasmon resonance (SPR) in a Biacore 3000 apparatus (Biacore AB). A goat anti-GST antibody was linked covalently to the carboxymethyldextran chip up to 6000 resonance units. Installations of GST–P fusion proteins (1 μM) were performed at an injection flow of 5 μl min^{-1} in HEPES buffer (pH 7.3), 0.15 M NaCl, until stabilization of the immobilization level (6–8 min). Under these conditions, different levels of fusion proteins were captured by the antibody, depending on the size of the P fragment. Relative molar ratios of P : PΔN161 : PΔN230 were 1 : 1.5 : 2 (taking into account their decreasing molecular masses). Regeneration of the anti-GST capture antibody was achieved by a 2 min injection of glycine buffer (pH 2.2). Serial dilutions of RNA–N were injected on the captured fusion proteins for 6 min at 31–500 nM and dissociation was registered for 10 min after the end of injections. Interaction kinetics were analysed with BIA2.24 software provided by Biacore AB.

RESULTS

Characterization of the P(Δ)–N protein complexes purified from bacteria

An N-binding domain has been localized at the C terminus of the RSV P protein by several groups (see Introduction). We have determined previously that the RSV P and N proteins, when co-expressed in *E. coli*, form complexes that can be co-purified (Castagné *et al.*, 2004). In order to determine whether the C-terminal region of RSV P is an RNA–N- or N°-binding region, a region of P encompassing aa 161–241 that does not contain the P oligomerization domain was fused to GST and co-expressed with RSV N in *E. coli*. GST–P and GST–PΔN161 were co-expressed with N in *E. coli* and the purified complexes were compared and analysed. The purification yields of GST–PΔN161–N complexes were much higher than for GST–P–N complexes, with corresponding yields of 60 and 8 mg protein (l bacterial culture)$^{-1}$, respectively. Each protein complex was purified to > 95 % homogeneity, as estimated by SDS-PAGE and Coomassie brilliant blue staining (Fig. 1). The proteins were separated from GST by thrombin cleavage with an efficiency of approximately 100 % for both GST–P and GST–PΔN161, the P, PΔN161 and N proteins being recovered in the supernatant (Fig. 1).

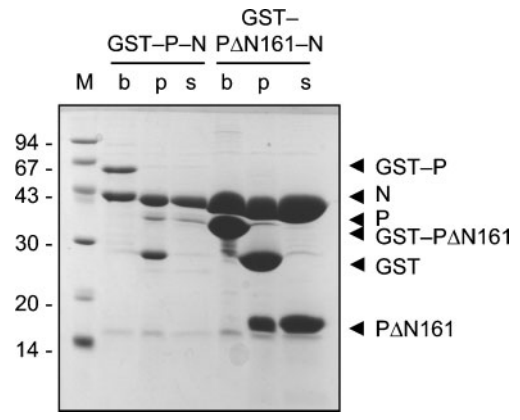

Fig. 1. SDS-PAGE analysis of GST–P–N and GST–PΔN161–N complexes purified from *E. coli*. Samples were denatured in Laemmli buffer, run on 12 % polyacrylamide gels and detected with Coomassie brilliant blue staining. To separate P and PΔN161–N from GST, complexes were incubated with thrombin overnight at 20 °C. After centrifugation, 10 μl beads/wash buffer (1 : 1) (v/v) (p) or supernatant (s) was loaded per lane together with uncleaved beads (b). M, Protein molecular size standards (kDa).

In order to characterize and compare the complexes co-purified by using either the oligomeric full-length P or the C-terminal fragment PΔN161, the samples were analysed by negative-staining electron microscopy (EM) after proteolytic separation from GST. Fig. 2(a, b) shows nucleocapsid-like structures eluted from GST beads for both P–N (a) and PΔN161–N (b). Interestingly, N-containing complexes purified by GST–PΔN161 comprised essentially ring-like structures, whilst those purified by GST–P contained essentially helices, along with some rings. The helical structures are morphologically identical to those isolated from HRSV virions and from infected cells. Furthermore, they look very similar to those described by Bhella *et al.* (2002) observed in insect cell-derived preparations produced by recombinant expression of RSV N with the baculovirus system.

In order to characterize and compare the purified P–N and PΔN161–N complexes further, the samples were analysed by size-exclusion chromatography on a Sephacryl S-300 (Amersham Biosciences) gel-filtration column (Fig. 2c) after filtering through a 0.22 μm pore-size filter immediately before loading. The apparent mass corresponding to each peak was estimated by the elution volume and calibration with known molecular mass standards. The collected fractions were analysed by EM and by SDS-PAGE and Coomassie blue staining. The identity of the polypeptides present in the different bands of the gel was determined by mass spectrometry (MALDI-TOF). The P–N sample eluted as a single major peak (P1) at 10.2 ml, with an apparent mass of about 700 kDa. The P and N proteins co-eluted from fractions 10 to 15 (Fig. 2d), indicating that only a high-molecular-mass complex containing the N and P proteins

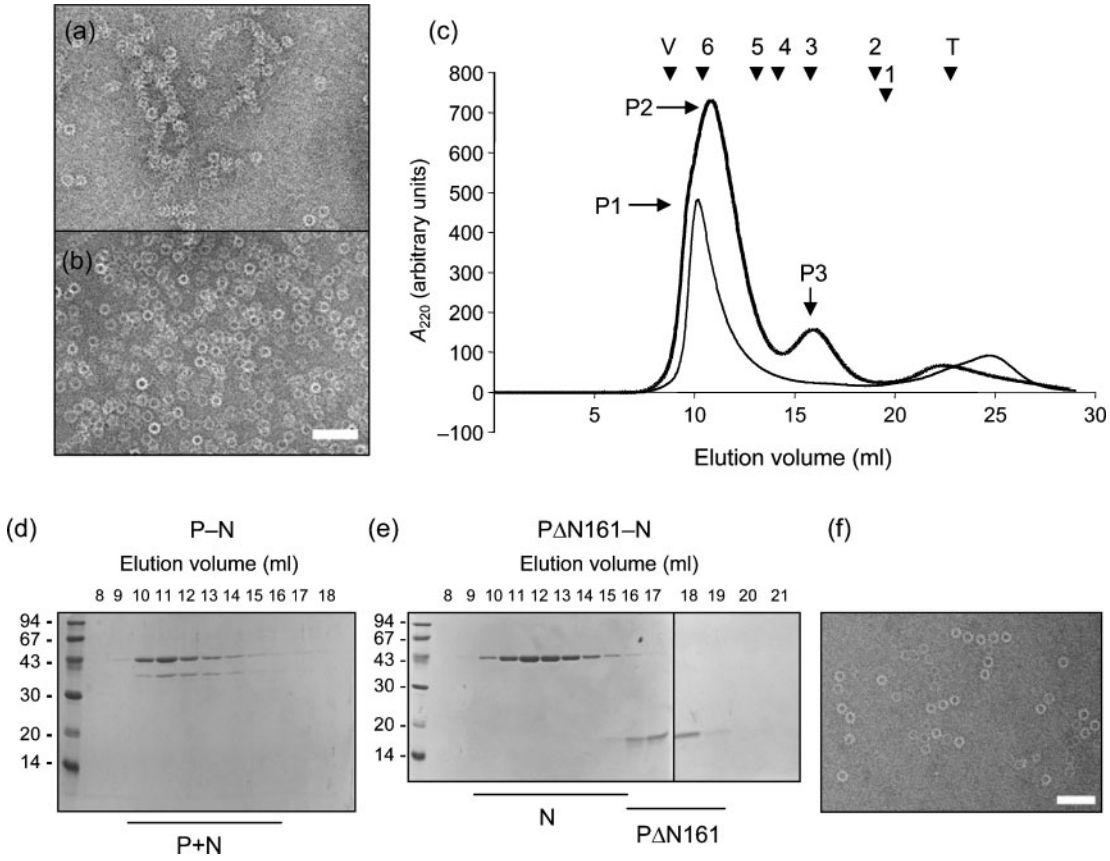

Fig. 2. Analysis of the different P–N complexes isolated from *E. coli* by EM and gel filtration. (a) Expression of full-length P and N and purification of GST–P–N complexes result in the purification of helical ribonucleoprotein complexes morphologically identical to RSV nucleocapsids, as well as some ring-like structures. (b) Purification of GST–PΔN161–N complexes leads to the production of essentially only ring-like structures, although a few short helices are sometimes seen. Bar, 50 nm. (c) Elution profiles of the P–N (thin line) and PΔN161–N (bold line) complexes. Absorbance was monitored at 220 nm. Samples (1 ml) were filtered through a 0.22 μm pore-size filter and run on a Sephacryl S300 column and fractions of 1 ml were collected. The following size markers (Amersham Biosciences) were used to calibrate the column (M_r in parentheses): 1, ribonuclease A (13 700); 2, chymotrypsinogen A (20 200); 3, ovalbumin (47 200); 4, albumin (61 000); 5, aldolase (176 000); 6, thyroglobulin (699 000). V, Void volume; T, total volume of the column. (d, e) Fractions (10 μl per lane) from P–N (d) and PΔN161 (e) were analysed by SDS-PAGE (10 % gel) and stained with Coomassie blue. (f) Samples from peaks P1 and P2 were observed by EM. Bar, 50 nm.

was present in the preparation. The PΔN161–N complexes showed a different profile, with two major peaks (Fig. 2c). The first peak (P2) eluted at 11.6 ml, with absorption detected at both 220 and 280 nm, and contained exclusively protein N (Fig. 2e). The size of this complex was estimated to be approximately 530 kDa from the Stokes radius. The second peak (P3), which eluted at 16.9 ml, only absorbed at 220 nm and contained the PΔN161 fragment. Its apparent mass was between 20.2 and 47.2 kDa, higher than its predicted mass of 10 kDa, presumably due to a markedly non-globular shape of the fragment (Tarbouriech *et al.*, 2000). The elution profiles of the shorter forms of P, such as PΔN220–N complexes, were similar to that of the PΔN161–N complexes (not shown). When the fractions were analysed by EM, the micrographs showed that only rings are visible in peaks P1 and P2 (Fig. 2f) and the amount of material was always less in the P–N sample.

These results showed that, after separation from GST and glutathione–Sepharose beads, the P–N complex remained associated during gel filtration, whereas PΔN161–N complexes dissociated.

Stability of P–RNA–N binding

For insight into the interaction stability of P-deletion mutants and RNA–N rings, binding kinetics were studied by SPR using Biacore technology. Fusion GST–P or GST–P fragments were immobilized by an anti-GST antibody and serial dilutions of N rings purified by gel filtration of PΔN161–N were injected. Typical SPR interaction sensorgrams are overlaid on Fig. 3. Computational analyses led to a complex model of interaction resulting from the N ring multi-valencies and potential steric hindrance. Nevertheless, qualitative information could be drawn from the dissociation phases (independent of the analyte concentration) about relative stabilities of the complexes, depending on the size of P fragments. A stable interaction between N and full-length P was observed, contrasting with the fair dissociation of PΔN230–N and the rapid dissociation of PΔN161–N. Indicative kinetic dissociation constants (k_{off}), assuming a simplified kinetic scheme, could be calculated (expressed in s^{-1}): 5.35×10^{-5} for P–N, 1.52×10^{-4} for PΔN230–N, 2.4×10^{-4} for PΔN161–N. These numbers have only an operational meaning and the latter accounts for the feasibility of separating RNA–N rings from PΔN161–N complexes by gel filtration.

Characterization of the RNA–N rings

The ring-like structures purified from the GST–PΔN161–N samples by gel filtration were analysed by EM imaging. Image analysis showed the presence of rings of different sizes. Visual inspection of the micrographs revealed that 10 or 11 spokes, 30 Å long, protrude from the continuous core of the structure, suggesting a ring composition of either 10 or 11 N proteins. By using the image-processing procedure described in Methods, we were able to confirm this observation and to distribute the rings in two classes, one having 10 and the other 11 radial projections. The dataset gave a final classification of 1120 particles matching the first model (decamers or 10N rings), with 681 particles matching the undecamer (11N rings) model. The average ring profiles indicate that the rings are roughly 12 and 14 nm in outer diameter for 10N and 11N rings, respectively, with each N subunit appearing as an elongated molecule of about 4.5 nm long (in the radial direction) and 2.5 nm across (Fig. 4a). The central holes of the rings have a diameter of about 4 and 5 nm, respectively, surrounded by an inner, high-density ring about 2 nm thick, from which 10 or 11 densities project radially by about 2.5 nm. This result is in agreement with previous analyses using recombinant baculovirus to produce RSV N in insect cells, which resulted in a mixture of helical and ring-like structures of 10 and 11 subunits (Bhella *et al.*, 2002). From our calculations, the majority are 10N rings ($\sim$62 %), whilst approximately 38 % are 11N rings.

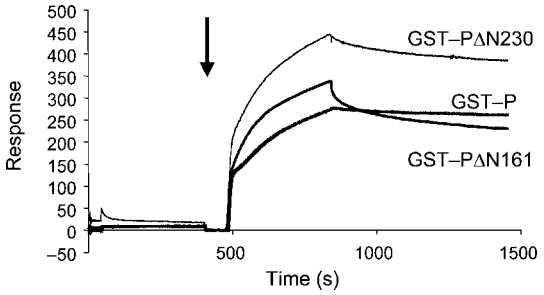

Fig. 3. Real-time kinetics of interaction between RNA–N rings and GST-P(Δ) fusion proteins. Overlay plot of sensorgrams corresponding to interaction of N protein with different GST-fusion proteins. GST-fusion proteins encompassing PΔN230, full-length P or PΔN161 were captured to saturation by anti-GST antibody linked covalently to the carboxymethyldextran chip. Then, N protein (125 nM) was injected for 6 min (arrow at the beginning of the N injection) and dissociation was followed for 10 min after the end of injection. RNA–N binding to full-length P is clearly more stable than binding to C-terminal fragments alone (compare slopes of the curves in the dissociation phase). Values obtained with non-specific interaction between RNA–N and GST alone were deduced from the curves.

The heterogeneity of the rings was investigated further by native PAGE. Samples containing PΔN161–N complexes were run on a 4 % polyacrylamide gel in 0.2 × TBE (pH 8.0) at 4 °C and stained with Coomassie blue. The nature of the polypeptides was determined by MALDI-TOF. As shown in Fig. 4(b, c), two bands were observed containing protein N. ImageJ software was used to estimate the relative amounts, yielding about 1 : 3 and 2 : 3 for the slower- and faster-migrating bands, respectively. By comparison with the EM data reported above, it is probable that the faster- and slower-migrating bands correspond to 10N and 11N rings, respectively.

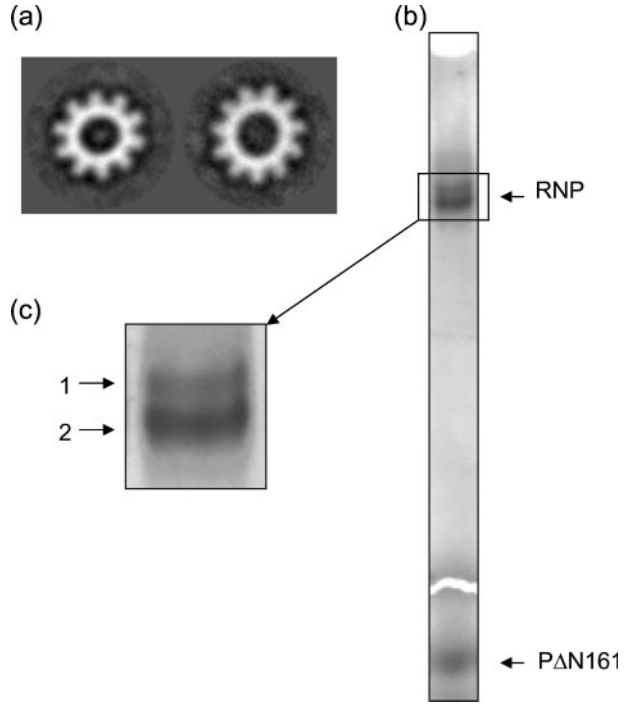

Fig. 4. Two types of ring are present in the PΔN161–N preparations. (a) Imaging of PΔ161N–N-derived ring structures embedded in 0.1 % trehalose produced high-quality images that were used to calculate two-dimensional top-view averages, revealing that approximately 62 % of RNA–N rings comprise 10 N monomers (left), whilst 38 % comprise 11 N monomers (right). (b) Analysis of PΔN161N–N complexes by native PAGE; (c) magnification of the bands containing N.

Characterization of the RNA present in the RNA–N ring-like complexes

The ring-like structures are believed to form by non-specific binding of N to cellular RNAs. In order to analyse the RNA content of the complexes, RNAs were phenol-extracted from 6 mg of a preparation of GST–PΔN161–N bound to Sepharose beads. A total of 60 μg pure RNA was obtained, corresponding to approximately 1 % of the mass of the complex. The length and the homogeneity of the RNA present in the complex were assessed by urea-PAGE using a 10 % polyacrylamide gel stained with ethidium bromide. As shown in Fig. 5(a), a doublet migrating with an apparent size of about 70 nt was observed, showing that *E. coli* RNAs were encapsidated by the RSV N protein in the presence of GST–P or GST–PΔN161.

The total extracted RNAs were analysed by MALDI-O-TOF mass spectrometry (Fig. 5b). In all cases, two broad peaks were detected clearly, with maxima at 23 550 and 25 480 Da. The width of these partially overlapping peaks indicates a heterogeneous composition and/or length of the encapsidated RNAs. To see whether these RNAs are protected from ribonuclease digestion within the rings, we treated the samples with RNase A and washed them extensively before phenol extraction. Fig. 5(c, d) shows the relevant section of a mass spectrum of the RNAs with or without RNase A treatment. The spectrum shows that nuclease digestion shifts the maxima toward lower values (22 900 and 24 820 Da). Most importantly, the peaks become narrower, suggesting that the rings protect two different lengths and that, prior to digestion, the complex may have overhanging RNA that is not protected. Although the mass assignment, particularly for the larger species, is less accurate due to the moderate mass resolution, the lengths of the RNA molecules in peaks 1 and 2 (corresponding to non-digested RNAs) can be estimated to 69.37 and 75.06 bases on average, respectively, using 339.455 Da as the mean mass of one ribonucleotide. After nuclease digestion, the estimated lengths become 67.5 and 73.12 bases, respectively. The reduced width of the peaks is compatible with heterogeneity in composition and a rather homogeneous length, suggesting that the two types of ring protect a defined length of

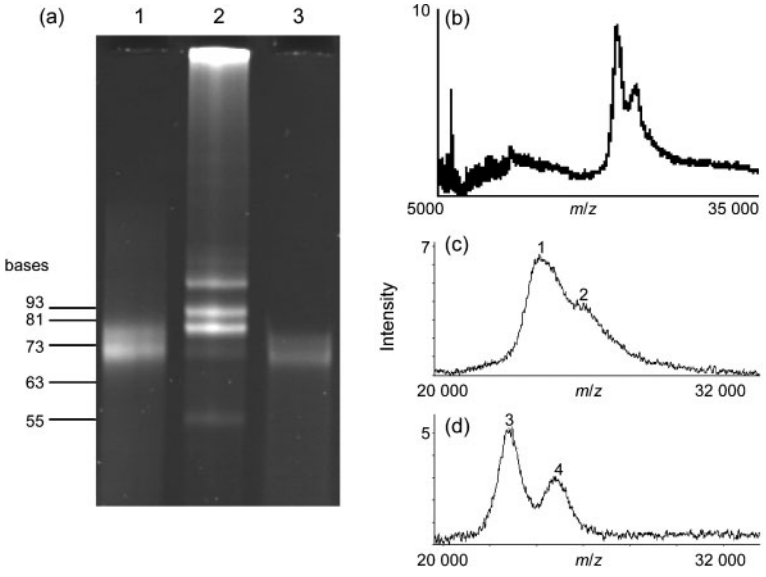

Fig. 5. Characterization of the RNA present in the RNA–N rings purified by GST–PΔN161. (a) RNA was phenol-extracted from beads containing GST–PΔN161–N complexes, run on a 10 % 8 M urea/polyacrylamide gel and stained with ethidium bromide. Lane 1, RNA from untreated beads; lane 2, RNA markers; lane 3, RNA from RNase A-treated beads. (b, c, d) MALDI-O-TOF mass spectra of RNA extracted from GST–PΔ161N–N complexes from untreated (b, c) or RNase A-treated (d) beads. Signals were magnified to compare spectra in (c) and (d). The calculated mean masses of the different peaks were: 1, 24 300 Da; 2, 25 920 Da; 3, 22 900 Da; 4, 24 820 Da.

cellular RNAs. Considering that rings are composed of 10N and 11N subunits, the expected lengths of the protected RNAs would be 60 and 66 bases if N contacted six ribonucleotides, and 70 and 77 bases if N contacted seven ribonucleotides. However, it is possible that the overhanging RNA cannot be digested exactly at the edge, leaving a few extra bases protected at the 5′ and 3′ ends of the RNA to which the nuclease may not have access in the ring. The most plausible interpretation of these data is that each N molecule contacts six ribonucleotides, and that three or four bases overhang at each end after digestion because they are protected from RNase within the ring.

Characterization of the minimal RNA–N-binding segment of P

To characterize further the P segment retaining an efficient RNA–N-binding ability as determined with our pull-down assays, a series of N-terminal deletions was done throughout the 161–241 region of P fused to GST. The ability of the GST–PΔ proteins to pull down RNA–N complexes was evaluated by SDS-PAGE and Coomassie blue staining of the purified complexes. Representative results are presented in Fig. 6. As seen in Fig. 6(b), an increase in the electrophoretic mobility of the GST–PΔ mutants was observed, as expected, depending on deletion size. The amounts of N pulled down by all N-terminal PΔN mutants of up to 229 aa – PΔN161, PΔN180, PΔN200, PΔN220N and PΔN230 – were equivalent to or higher than those obtained by using full-length P, as estimated by Coomassie blue staining. No N was pulled down by GST alone, nor by P mutants retaining the central region (P82–208), which contains the oligomerization domain of P (Castagné *et al.*, 2004; Llorente *et al.*, 2006), nor the 1–40 region. P160–230, which lacks the last 11 residues, was also unable to pull down N. Interestingly, a dramatic change in the apparent molecular mass on SDS-PAGE was observed between GST–PΔN200 and GST–PΔN220, suggesting that the 200–220 region of P is responsible for the abnormal SDS-PAGE migration of the RSV P protein, which has a predicted mass of 27 kDa, but migrates with an apparent mass of approximately 35 kDa (Mazumder *et al.*, 1994). Analysis of the complexes purified by GST–PΔN230 by EM and gel filtration revealed that they are similar to those purified by GST–PΔN161 (not shown). Together, these results therefore indicate clearly that the last C-terminal 12 aa of P by themselves constitute a strong RNA–N-binding site.

We then shortened the P230–241 region at either end and produced the corresponding GST–P proteins in *E. coli*. Mutants PΔN231, PΔN232 and PΔN233 – the latter retaining only the nine most C-terminal amino acids of P – were still able to pull down N with the same efficiency as PΔN230 (Fig. 6c, d). We were unable to purify the PΔN234–N complex (retaining only the eight C-terminal amino acids), but additional truncations, like in PΔN235 and PΔN236, led to recovery of very small amounts of pulled-down N, which became undetectable with the further deletion constructs (PΔN237 to PΔN241, the latter containing only one residue, Phe). On the other hand, removal of the very C-terminal amino acid of P completely abolished its capacity to pull down N, just like the other mutants tested lacking 2 or 3 aa

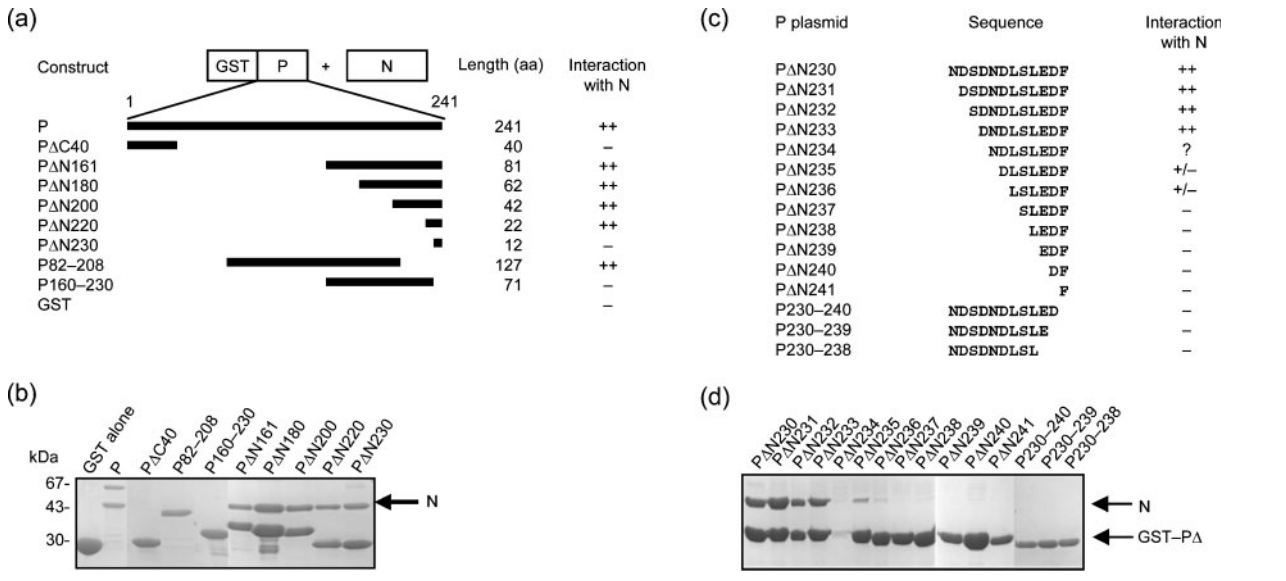

Fig. 6. Mapping of ribonucleoprotein-binding region of RSV P by deletions. (a) Schematic representation and (c) sequence of the P-deletion mutants fused to GST that were co-expressed in *E. coli* together with N for GST pull-down assays. (c) PΔN230 corresponds to the last 12 C-terminal residues of P. The right-hand columns in (a) and (c) summarize interactions between GST–P mutants and His–N shown in (b) and (d), respectively. (b, d) Coomassie blue-stained SDS-PAGE of GST-pulled-down complexes.

from the C terminus (Fig. 6c, d). Thus, the C-terminal P segment spanning aa 234–241 appears to contain the minimal region for efficient interaction with RNA–N in this system. We have not investigated the effect of removing just these amino acids in the context of full-length P, but these results argue strongly in favour of this conclusion.

The amino acid sequence of RSV P between residues 231 and 241 is relatively hydrophilic, containing eight polar side chains of which five are acidic (Glu and Asp), with no basic residue to compensate the electrostatic charge, so that this peptide is highly negatively charged. We substituted each amino acid individually with Ala in the GST-fusion construct of the peptide to assess the effect on RNA–N binding. As shown in Fig. 7(a), substitutions of Leu^{238} and Phe^{241} by Ala abrogated P–N binding, whereas single substitutions at the other residues had no visible effect, indicating that Leu^{238} and Phe^{241} appear to play a critical role in the P–RNA–N interaction. Substitution of Phe^{241} by Trp restored the interaction (Fig. 7a), indicating that an aromatic residue is necessary at the C terminus of P for P–N interaction. Thus, in this polar peptide, two of the three non-polar residues present are important for binding. Although a single substitution of the acidic residues had no apparent effect, the mutant PΔN231–DE/A, in which all negatively charged residues were changed to Ala, lost the ability to bind RNA–N, indicating that negative charges play a role in the RNA–N–P interaction in a cooperative manner. An interesting locus is Ser^{232}, which is the main phosphorylation site of P (Sánchez-Seco *et al.*, 1995). We observed no effect when substituting Ser^{232} to Ala, Asp or Glu (the latter two side chains were chosen to mimic the negative charge resulting from phosphorylation at this position). These results suggest that phosphorylation of Ser^{232} does not affect the interaction of P with RNA–N.

To investigate the possibility that the very C terminus of P might insert into a matching cavity in N, we tested whether the addition of extra amino acids at the C terminus of P would abrogate the interaction. Fig. 7(b) shows that it is probably not the case because, except for Ala, addition of one or two residues at the C terminus of PΔN231 did not affect the interaction, using either single or double aromatic (Phe, Tyr) or acidic (Asp) residues.

	P plasmid	Sequence	Interaction with N
(a)	PΔN231	DSDNDLSLEDF	+
	PΔN231-S232A	-A---------	+
	PΔN231-D233A	--A--------	+
	PΔN231-N234A	---A-------	+
	PΔN231-L236A	----A------	+
	PΔN231-S237A	-----A-----	+
	PΔN231-L238A	------A----	+
	PΔN231-E239A	-------A---	–
	PΔN231-D240A	--------A--	+
	PΔN231-F241A	---------A-	+
	PΔN231-F241W	----------A	–
	PΔN231-F241D	----------W	+
	PΔN231-DE/A	----------D	–
	PΔN231-S232A	A-A-A---AA-	–
	PΔN231-S232E	-A---------	+
	PΔN231-S232D	-E---------	+
		-D---------	+
(b)	PΔN231	DSDNDLSLEDF	+
	PΔN231-242A	----------A	–
	PΔN231-242Y	----------Y	+
	PΔN231-242D	----------D	+
	PΔN231-242F	----------F	+
	PΔN231-242AA	----------AA	–
	PΔN231-242DD	----------DD	+
	PΔN231-242FF	----------FF	+

Fig. 7. Analysis of the RNA–N-binding ability of mutated PΔN231 region by GST pull-down assays as described in the legend to Fig. 6. (a) Effect of point mutations. (b) Effect of the addition of residues at the C terminus of PΔN231. Sequences of the different peptides fused in frame at the C terminus of GST are shown. The right-hand column indicates the presence (+) or absence (–) of N in the purified complexes.

DISCUSSION

In the present work, we have analysed the nature of the P–N complexes purified from *E. coli* by using full-length or truncated forms of P fused to GST and co-expressed with N. We observed that different RNA–N complexes were pulled down by GST–P and by the GST–PΔN161 fragment, which corresponds to the C-terminal region of P devoid of the oligomerization domain. The RNA–N complexes observed when using intact P resembled those observed previously when expressing recombinant N by itself, with a majority of helical structures and a few rings. In contrast, those obtained with the C-terminal fragment of P (mutant GST–PΔN161) consisted essentially of rings. Differences at the quantitative level were also observed: the purification yields for the GST–PΔN161–N complex were about sevenfold higher than those for the GST–P–N complex. These differences will need further experiments to be elucidated.

The electron micrographs of RNA–N preparations purified with GST–PΔN161–N show clearly that some rings have 10 and others have 11 projections, which are visible by eye. Computational analysis confirmed this observation, revealing that about one-third of the rings were 11N and two-thirds were 10N. We have previously observed the presence of these two types of ring in preparations of recombinant N in the absence of P (Bhella *et al.*, 2002). However, in these preparations, the majority of N was in the form of helical RNA–N complexes. In this report, we provide statistically robust data suggesting that these are the two preponderant types of rings present, if not the only ones. Furthermore, analysis of the length of the protected RNA molecules revealed two peaks, consistent with the presence of two types of structure. It can be concluded that the 10N and 11N rings are the overwhelming majority of the rings produced and that any other minor forms, if present, are not detected with our assays.

The rings that we have examined correspond to non-specific encapsidation of cellular RNAs by N. However, because in the complex there are specific lateral interactions between adjacent N protomers, leaving a fixed spacing between RNA-binding sites, it is expected that each N molecule will contact a fixed number of ribonucleotides, as it is the case for other paramyxoviruses. Our analysis of the RNAs extracted from the rings revealed an apparent heterogeneity in length and composition. Furthermore, our data indicated that the two different types of ring protect different lengths of RNA from RNase A digestion. An average of 67 and 73 bases was protected by the N decamers and undecamers, respectively, i.e. 6.7 per protomer for both structures. The resulting numbers can be interpreted as six protected ribonucleotides per protomer in the 10N and 11N rings, with an additional three or four bases protected from the nuclease at the 5′ and 3′ ends. Although RSV does not follow the rule of six (Samal & Collins, 1996), the first RSV genome sequence – from which an infectious cDNA was obtained – happened to contain a multiple of six (Collins *et al.*, 1995). It was shown, however, that addition of one to five extra bases at the end of minigenomes did not affect their replication ability, when minigenomes containing heterologous extensions of 6 nt or more were unable to support efficient RNA synthesis (Cowton & Fearns, 2005). A survey of the human and bovine RSV genomic sequences available now in GenBank shows that most of them are not multiples of six. Similarly, the N proteins from rhabdoviruses were shown to contact nine ribonucleotides, with no requirement to have a genome length as a multiple of nine for efficient replication (Kolakofsky *et al.*, 2005).

In order to map and characterize this region on the P protein, truncated forms of the P protein fused to GST were tested for their ability to pull down the N protein from bacterial lysates. Surprisingly, when reduced to the nine most C-terminal residues fused to GST, this region was still able to interact with RNA–N complexes with a high efficiency. As there is no phosphorylation of RSV P in bacteria (Castagné *et al.*, 2004), these results also demonstrate that interaction of P with RNA–N does not depend on P phosphorylation. These variations in the detection of P–N interactions might be related to the techniques used. For example, G172S and E176G temperature-sensitive mutations on the P protein affected P–N interaction as assayed by the two-hybrid system, but not by co-immunoprecipitation (Lu *et al.*, 2002). Furthermore, most of these experiments used internal deletions and fusion of normally separated regions that could result in abnormal conformation of the resulting fusion proteins.

The role of each amino acid in RNA–N–P interaction was investigated in the context of the peptide P231–241 fused to GST by mutagenesis. We found that substitution at residues Leu^{238} and Phe^{241} was highly inhibitory to P–N interaction, while other single substitutions affected binding to N poorly. However, substitution of all of the acidic residues present in this region abolished this interaction. These results indicated that there is not a strict requirement for all HRSV P protein C-terminal residues for interacting with N, but that acidic and hydrophobic residues (Leu^{238} and Phe^{241}) are critical for this interaction. In contrast, Slack & Easton (1998), using the yeast two-hybrid system, found that Ser^{232} and Ser^{237} substitution by Ala resulted in a twofold reduction in P–N interaction. By using co-immunoprecipitation experiments, Khattar *et al.* (2001b) observed that substitution mutations to Ala at positions N234, L236, L238, D240 or F241 of the bovine RSV P protein produced a tenfold reduction in binding to N. These authors used full-length P molecules and it is possible that these differences are due to the presence of 'negative-regulatory regions' situated upstream from the RNA–N-binding region, as proposed by Slack & Easton (1998). It is also possible that our method is less sensitive to mutations affecting non-essential residues for P–N interaction, due to a high local concentration of P on Sepharose beads.

Compared with nucleocapsid-binding domains of P proteins of members of the *Paramyxovirinae* [e.g. *Measles virus* (MV), SeV, *Mumps virus*] and *Rhabdoviridae* (RV), the RNA–N-binding region of RSV P appears profoundly different at the structural level (Fig. 8). The RNA–N-binding domains of SeV, MV and mumps virus P proteins, also called X-domains, consist of globular regions of about 50–100 residues and contain several α-helices (Curran *et al.*, 1995; Johansson *et al.*, 2003; Blanchard *et al.*, 2004; Kingston *et al.*, 2004). The structure of the RNA–N-binding domain of the rhabdovirus P protein is unrelated to those of SeV and

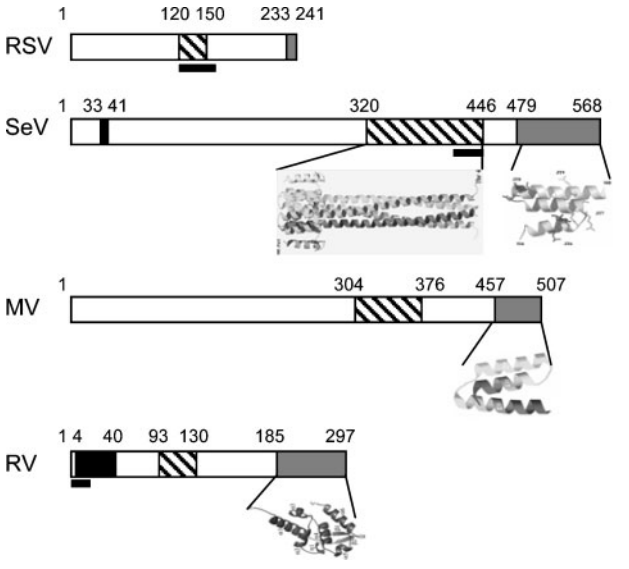

Fig. 8. Structural organization of RSV P and comparison with MV, SeV and RV P proteins. Amino acid residues are numbered. Grey boxes correspond to RNA–N-binding sites, hatched boxes to oligomerization (coiled-coil) domains and black boxes to N°-binding sites. L-binding regions are indicated by black bars. Structures that have been resolved at the atomic level are represented by small pictures positioned on the molecules.

MV RNA–N-binding domains and consists of 111 residues that fold into a single, compact domain including six α-helices and two β-sheets (Mavrakis *et al.*, 2004). Structural predictions on the RSV P protein and circular dichroism spectra of peptide 230–241 and region 161–241 indicated the absence of secondary structures (data not shown). Together, these data show that the structure of the C-terminal region of RSV P is unrelated to those of SeV, MV or RV P, indicating that they have diverged profoundly or that they do not come from the same evolutionary lineage.

ACKNOWLEDGEMENTS

We thank Céline Henry and Alain Guillot (INRA, Jouy-en-Josas, France) for mass spectrometry, Mohamed Moudjou for technical help and Jean Lepault for EM observations and helpful discussions.

REFERENCES

Asenjo, A. & Villanueva, N. (2000). Regulated but not constitutive human respiratory syncytial virus (HRSV) P protein phosphorylation is essential for oligomerization. *FEBS Lett* **467**, 279–284.

Barik, S., McLean, T. & Dupuy, L. C. (1995). Phosphorylation of Ser^{232} directly regulates the transcriptional activity of the P protein of human respiratory syncytial virus: phosphorylation of Ser^{237} may play an accessory role. *Virology* **213**, 405–412.

Bhella, D., Ralph, A., Murphy, L. B. & Yeo, R. P. (2002). Significant differences in nucleocapsid morphology within the *Paramyxoviridae*. *J Gen Virol* **83**, 1831–1839.

Blanchard, L., Tarbouriech, N., Blackledge, M., Timmins, P., Burmeister, W. P., Ruigrok, R. W. H. & Marion, D. (2004). Structure and dynamics of the nucleocapsid-binding domain of the Sendai virus phosphoprotein in solution. *Virology* **319**, 201–211.

Castagné, N., Barbier, A., Bernard, J., Rezaei, H., Huet, J.-C., Henry, C., Da Costa, B. & Eléouët, J.-F. (2004). Biochemical characterization of the respiratory syncytial virus P–P and P–N protein complexes and localization of the P protein oligomerization domain. *J Gen Virol* **85**, 1643–1653.

Collins, P. L., Hill, M. G., Camargo, E., Grosfeld, H., Chanock, R. M. & Murphy, B. R. (1995). Production of infectious human respiratory syncytial virus from cloned cDNA confirms an essential role for the transcription elongation factor from the 5′ proximal open reading frame of the M2 mRNA in gene expression and provides a capability for vaccine development. *Proc Natl Acad Sci U S A* **92**, 11563–11567.

Collins, P. L., Chanock, R. M. & Murphy, B. R. (2001). Respiratory syncytial virus. In *Fields Virology*, 4th edn, pp. 1443–1485. Edited by D. M. Knipe & P. M. Howley. Philadelphia, PA: Lippincott Williams & Wilkins.

Conway, J. F. & Steven, A. C. (1999). Methods for reconstructing density maps of ''single'' particles from cryoelectron micrographs to subnanometer resolution. *J Struct Biol* **128**, 106–118.

Cowton, V. M. & Fearns, R. (2005). Evidence that the respiratory syncytial virus polymerase is recruited to nucleotides 1 to 11 at the 3′ end of the nucleocapsid and can scan to access internal signals. *J Virol* **79**, 11311–11322.

Curran, J., Marq, J.-B. & Kolakofsky, D. (1995). An N-terminal domain of the Sendai paramyxovirus P protein acts as a chaperone for the NP protein during the nascent chain assembly step of genome replication. *J Virol* **69**, 849–855.

García, J., García-Barreno, B., Vivo, A. & Melero, J. A. (1993). Cytoplasmic inclusions of respiratory syncytial virus-infected cells: formation of inclusion bodies in transfected cells that coexpress the nucleoprotein, the phosphoprotein, and the 22K protein. *Virology* **195**, 243–247.

García-Barreno, B., Delgado, T. & Melero, J. A. (1996). Identification of protein regions involved in the interaction of human respiratory syncytial virus phosphoprotein and nucleoprotein: significance for nucleocapsid assembly and formation of cytoplasmic inclusions. *J Virol* **70**, 801–808.

Grosfeld, H., Hill, M. G. & Collins, P. L. (1995). RNA replication by respiratory syncytial virus (RSV) is directed by the N, P, and L proteins; transcription also occurs under these conditions but requires RSV superinfection for efficient synthesis of full-length mRNA. *J Virol* **69**, 5677–5686.

Johansson, K., Bourhis, J.-M., Campanacci, V., Cambillau, C., Canard, B. & Longhi, S. (2003). Crystal structure of the measles virus phosphoprotein domain responsible for the induced folding of the C-terminal domain of the nucleoprotein. *J Biol Chem* **278**, 44567–44573.

Khattar, S. K., Yunus, A. S. & Samal, S. K. (2001a). Mapping the domains on the phosphoprotein of bovine respiratory syncytial virus required for N–P and P–L interactions using a minigenome system. *J Gen Virol* **82**, 775–779.

Khattar, S. K., Yunus, A. S., Collins, P. L. & Samal, S. K. (2001b). Deletion and substitution analysis defines regions and residues within the phosphoprotein of bovine respiratory syncytial virus that affect transcription, RNA replication, and interaction with the nucleoprotein. *Virology* **285**, 253–269.

Kingston, R. L., Hamel, D. J., Gay, L. S., Dahlquist, F. W. & Matthews, B. W. (2004). Structural basis for the attachment of a paramyxoviral polymerase to its template. *Proc Natl Acad Sci U S A* **101**, 8301–8306.

Kolakofsky, D., Le Mercier, P., Iseni, F. & Garcin, D. (2004). Viral DNA polymerase scanning and the gymnastics of Sendai virus RNA synthesis. *Virology* **318**, 463–473.

Kolakofsky, D., Roux, L., Garcin, D. & Ruigrok, R. W. H. (2005). Paramyxovirus mRNA editing, the 'rule of six' and error catastrophe: a hypothesis. *J Gen Virol* **86**, 1869–1877.

Llorente, M. T., García-Barreno, B., Calero, M., Camafeita, E., López, J. A., Longhi, S., Ferrón, F., Varela, P. F. & Melero, J. A. (2006). Structural analysis of the human respiratory syncytial virus phosphoprotein: characterization of an α-helical domain involved in oligomerization. *J Gen Virol* **87**, 159–169.

Loboda, A. V., Ackloo, S. & Chernushevich, I. V. (2003). A high-performance matrix-assisted laser desorption/ionization orthogonal time-of-flight mass spectrometer with collisional cooling. *Rapid Commun Mass Spectrom* **17**, 2508–2516.

Longhi, S., Receveur-Bréchot, V., Karlin, D., Johansson, K., Darbon, H., Bhella, D., Yeo, R., Finet, S. & Canard, B. (2003). The C-terminal domain of the measles virus nucleoprotein is intrinsically disordered and folds upon binding to the C-terminal moiety of the phosphoprotein. *J Biol Chem* **278**, 18638–18648.

Lu, B., Brazas, R., Ma, C.-H., Kristoff, T., Cheng, X. & Jin, H. (2002). Identification of temperature-sensitive mutations in the phosphoprotein of respiratory syncytial virus that are likely involved in its interaction with the nucleoprotein. *J Virol* **76**, 2871–2880.

Ludtke, S. J., Baldwin, P. R. & Chiu, W. (1999). EMAN: semiautomated software for high-resolution single-particle reconstructions. *J Struct Biol* **128**, 82–97.

Mallipeddi, S. K., Lupiani, B. & Samal, S. K. (1996). Mapping the domains on the phosphoprotein of bovine respiratory syncytial virus required for N–P interaction using a two-hybrid system. *J Gen Virol* **77**, 1019–1023.

Mason, S. W., Aberg, E., Lawetz, C., DeLong, R., Whitehead, P. & Liuzzi, M. (2003). Interaction between human respiratory syncytial virus (RSV) M2-1 and P proteins is required for reconstitution of M2-1-dependent RSV minigenome activity. *J Virol* **77**, 10670–10676.

Mavrakis, M., McCarthy, A. A., Roche, S., Blondel, D. & Ruigrok, R. W. H. (2004). Structure and function of the C-terminal domain of the polymerase cofactor of rabies virus. *J Mol Biol* **343**, 819–831.

Mavrakis, M., Méhouas, S., Réal, E., Iseni, F., Blondel, D., Tordo, N. & Ruigrok, R. W. H. (2006). Rabies virus chaperone: identification of the phosphoprotein peptide that keeps nucleoprotein soluble and free from non-specific RNA. *Virology* **349**, 422–429.

Mazumder, B., Adhikary, G. & Barik, S. (1994). Bacterial expression of human respiratory syncytial viral phosphoprotein P and identification of Ser^{237} as the site of phosphorylation by cellular casein kinase II. *Virology* **205**, 93–103.

Navarro, J., López-Otín, C. & Villanueva, N. (1991). Location of phosphorylated residues in human respiratory syncytial virus phosphoprotein. *J Gen Virol* **72**, 1455–1459.

Samal, S. K. & Collins, P. L. (1996). RNA replication by a respiratory syncytial virus RNA analog does not obey the rule of six and retains a nonviral trinucleotide extension at the leader end. *J Virol* **70**, 5075–5082.

Sánchez-Seco, M. P., Navarro, J., Martínez, R. & Villanueva, N. (1995). C-Terminal phosphorylation of human respiratory syncytial virus P protein occurs mainly at serine residue 232. *J Gen Virol* **76**, 425–430.

Slack, M. S. & Easton, A. J. (1998). Characterization of the interaction of the human respiratory syncytial virus phosphoprotein and nucleocapsid protein using the two-hybrid system. *Virus Res* **55**, 167–176.

Tarbouriech, N., Curran, J., Ruigrok, R. W. H. & Burmeister, W. P. (2000). Tetrameric coiled coil domain of Sendai virus phosphoprotein. *Nat Struct Biol* **7**, 777–781.